

## Detection of temperature- and stress-induced modifications of $\text{LaCoO}_3$ by micro-Raman spectroscopy

Nina Orlovskaya,<sup>1,\*</sup> David Steinmetz,<sup>1</sup> Sergey Yarmolenko,<sup>2</sup> Devdas Pai,<sup>2</sup> Jag Sankar,<sup>2</sup> and John Goodenough<sup>3</sup>

<sup>1</sup>*Department of Materials Science and Engineering, Drexel University, Philadelphia, Pennsylvania 19104, USA*

<sup>2</sup>*Center for Advanced Materials and Smart Structures, North Carolina A&T State University, Greensboro, North Carolina 27411, USA*

<sup>3</sup>*Texas Materials Institute, The University of Texas at Austin, Austin, Texas 78712, USA*

(Received 30 June 2004; revised manuscript received 15 November 2004; published 21 July 2005)

Micro-Raman spectroscopy of  $\text{LaCoO}_3$ -based perovskites was performed to characterize the vibrational properties of these Raman active rhombohedral perovskites and their temperature and stress induced changes. The cobaltite spectra were found to consist of four Raman active phonon modes at 162, 448, 557, and 673  $\text{cm}^{-1}$  in the case where the laser power had been 2.5 mW. The two vibrational modes at 557 and 673  $\text{cm}^{-1}$  disappear at the semiconductor/metal transition at 500 K driven by laser overheating during a collection of the Raman signal at higher laser power. Significant stress-induced changes in the Raman spectrum of  $\text{LaCoO}_3$  after indentation were also observed. An increase of the intensities of two 557 and 670  $\text{cm}^{-1}$  bands at the center of an indentation correlated with evidence of a tensile stress created by a deformation of perovskite during indentation. The tensile stress stabilizes the state with longer mean Co-O bond length. The 448  $\text{cm}^{-1}$  band was found to be stress sensitive, therefore it was used for mapping of the residual stresses induced in the material by indentation. A qualitative estimate of the sign of the residual stress distribution after the indentation in  $\text{LaCoO}_3$  perovskite is presented.

DOI: 10.1103/PhysRevB.72.014122

PACS number(s): 78.30.Hv

### I. INTRODUCTION

$\text{LaCoO}_3$  is the parent compound of the  $\text{La}_{1-x}\text{Sr}_x\text{CoO}_{3-\delta}$  system that is a mixed electronic and oxide-ion conductor of technical interest for oxygen separation membranes, the cathode of solid oxide fuel cells, oxygen sensors, and catalysis.  $\text{LaCoO}_3$  itself is of fundamental interest because the Co(III) ions undergo a transition with increasing temperature from the low-spin (LS) state  $t^6e^0$  to the intermediate spin (IS) state  $t^5e^1$  in the temperature range  $35 \text{ K} < T < 320 \text{ K}$  to a conductive state near 500 K in which conductive electrons occupy itinerant-electron states of a  $\sigma^*$  band of  $e$ -orbital parentage.<sup>1</sup> The insulator-metal transition does not appear to be a homogeneous thermally induced Mott-Hubbard transition; rather the introduction of high-spin (HS) Co(III) creates conductive clusters that grow with increasing temperature to beyond percolation near 500 K.<sup>2</sup> The introduction of Sr in  $\text{La}_{1-x}\text{Sr}_x\text{CoO}_3$  creates hole-rich, conductive ferromagnetic clusters that have an IS configuration  $t^5\sigma^{*1-x}$  with  $x \approx 0.4$  and they grow with increasing  $x$  to beyond percolation.<sup>1</sup>

A measure of the mismatch of the equilibrium (La-O) and (Co-O) bond lengths in the cubic perovskite structure is the geometric tolerance factor  $t \equiv (\text{La-O})/[\sqrt{2}(\text{Co-O})]$ , where La-O and Co-O are the equilibrium bond length. A distortion from cubic  $Pm\bar{3}m$  to rhombohedral  $R\bar{3}c$  symmetry just below the melting point (1640 °C)<sup>3</sup> is induced by a tolerance factor  $t < 1$ . In  $\text{LaCoO}_3$ , the structure adjusts to a  $t < 1$  by a cooperative rotation of the  $\text{CoO}_{6/2}$  octahedra about a  $\langle 111 \rangle$  axis to give the rhombohedral  $R\bar{3}c$  structure. A strong evidence of the existence of the  $I2/a$  monoclinic distortion in the LS-IS state of  $\text{LaCoO}_3$  in the interval of  $40 \text{ K} < T < 500 \text{ K}$  were recently provided in Ref. 4.

Raman spectroscopy is a powerful tool for a study of various vibrational modes and electronic transitions in

solids.<sup>5</sup> It is particularly appropriate where dynamic local distortions occur that cannot be detected by a diffraction experiment. Such dynamic, local site distortions may be associated with the IS state Co(III):  $t^5e^1$  in  $\text{LaCoO}_3$ ; the IS Co(III) is a strong Jahn-Teller (JT) ion. The crystal structure changes from rhombohedral to monoclinic phase by the cooperative JT effect in a certain temperature range.<sup>4</sup> Local  $I2/a$  monoclinic distortion in  $\text{LaCoO}_3$  was also detected by micro-Raman.<sup>6</sup> Local  $E_g$  vibrational modes would distinguish the IS Co(III) from the HS Co(III):  $t^4e^2$  or an IS Co(III):  $t^5\sigma^{*1}$  having itinerant electrons in a  $\sigma^*$  band of  $e$ -orbital parentage. Although several recent publications<sup>7-10</sup> have reported Raman spectra for the perovskite  $\text{LaMnO}_3$ , only a few papers have recently appeared dealing with  $\text{LaCoO}_3$  based perovskites.<sup>6,11,12</sup> The reasons for this are as follows:

(1) The nearly cubic structure of the doped lanthanum cobaltite materials renders first-order Raman scattering extremely weak; therefore, a long time is needed for spectra collection.

(2) The small penetration depth of the excitation radiation also results in a decrease of the scattering intensity.

(3) Microinhomogeneous areas exist at the perovskite surface, which makes it difficult to interpret the results.

(4) Undesired/desired laser-induced heating of the cobaltite surface occurs during collection of spectra. To avoid overheating, one needs to limit the power of the laser excitation. To induce heating, one needs to use maximum laser power.

In the ideal cubic perovskite structure, all lattice sites have inversion symmetry. Therefore, first-order Raman scattering is forbidden.  $\text{LaCoO}_3$  belongs to the family of rotationally distorted perovskites,<sup>13</sup> and its structure can be obtained by rotation of the adjacent  $\text{CoO}_{6/2}$  octahedra in

opposite directions around the  $[111]_c$  direction of the ideal cubic structure. The La atoms occupy the  $2a$   $(1/4, 1/4, 1/4)$  positions and participate in four  $A_{2g} + A_{2u} + E_g + E_u$  phonon modes. The Co atoms occupy the  $2b$   $(0, 0, 0)$  positions and participate in  $A_{1u} + A_{2u} + 2E_u$  phonon modes. The oxygen atoms occupy the  $6e$   $(x, \bar{x} + 1/2, 1/4)$  and participate in  $A_{1g} + A_{1u} + 2A_{2g} + 2A_{2u} + 3E_g + 3E_u$  phonon modes.

Factor group analysis of rhombohedral perovskites results in five Raman active phonon modes of irreducible representation  $A_{1g} + 4E_g$ .<sup>14</sup> The Raman active modes are associated with  $R$   $(1/2, 1/2, 1/2)$  point Brillouin zone boundary modes in the cubic phase, which become zone center modes because the Brillouin zone is halved in the rhombohedral phase.<sup>15,16</sup>

This paper presents the analysis of the experimental Raman spectra of pure  $\text{LaCoO}_3$  as a function of laser power and applied stress. The appearance of two  $557$  and  $673$   $\text{cm}^{-1}$  modes are assigned to the semiconducting state of  $\text{LaCoO}_3$ ; the disappearance of these modes about  $500$  K is associated with the temperature induced semiconductor to metal transition. The Stokes/anti-Stokes band ratio is used to calculate the temperature of the perovskite surface under laser heating. Stress-induced changes in  $\text{LaCoO}_3$  Raman spectra obtained with an indentation technique as well as the qualitative determination of the sign of the residual stresses in indented  $\text{LaCoO}_3$  are also reported.

## II. EXPERIMENTAL TECHNIQUES

A micro-Raman spectrometer Renishaw 1000 was used to study the vibrational spectra of the  $\text{LaCoO}_3$  based perovskites. The Raman microscope system comprises a laser ( $514.5$  nm line of  $\text{Ar}^+$  ion laser) to excite the sample, a single spectrograph fitted with holographic notch filters, and an optical microscope (a Leica microscope with a motorized XYZ mapping stage) rigidly mounted and optically coupled to the spectrograph.<sup>17</sup> The maximum generated laser power was  $25$  mW. For different measurements  $10\%$ ,  $25\%$ ,  $50\%$ , and  $100\%$  of the laser power were used. The average collection time for a single spectrum varied from  $200$  to  $500$  s per point. A plasma filter was used to remove plasma lines from the spectra taken. The incident and scattered beams were focused with a microscope having a  $100\times$  objective, which allowed keeping a laser spot as low as  $1\text{--}2$   $\mu\text{m}$ . All measurements were performed at room temperature. Before the  $\text{LaCoO}_3$  measurements, the spectrometer was calibrated with a Si standard using a Si band position at  $520.3$   $\text{cm}^{-1}$ .

Fully dense, single-phase polycrystalline  $\text{LaCoO}_3$  and  $\text{La}_{0.8}\text{Sr}_{0.2}\text{CoO}_3$  perovskites with a grain size of  $2\text{--}4$   $\mu\text{m}$  were used for measurements. Both perovskite materials were produced by Praxair, Inc. Raman scattering was performed on a mechanically polished ( $1$   $\mu\text{m}$  diamond) surface. The Vickers indentation ( $500$  g) was done to introduce an impression on the surface; a Nanoindenter XP equipped with a Berkovich pyramid was used to perform the nanoindentation tests. Different points of interest on the surface have been chosen, such as the polished surface, points inside the Vickers impression, points at the cracks originating from the corner of the impression, and points near the impression. The positions of the Raman bands are sample sensitive and vary

within  $10\text{--}15$   $\text{cm}^{-1}$  from the spectra of polycrystalline samples because of the existence of local chemical inhomogeneities in the samples. The area mapping was conducted with a laser having a spot size of  $1$   $\mu\text{m}$ . Autofocusing was used to collect the Raman spectra because it maintains a good focus on the sample during line/area confocal mapping experiments. To produce one-dimensional (1D) and two-dimensional (2D) maps, GRAMS and RENISHAW WIRE software with a mixed Lorentzian and Gaussian peak fitting function was used. The system was set up to take spectra from all points along a single line of interest on the surface or inside the selected area of interest. Peak positions determined by peak fitting were plotted to create a strain map with a spectral resolution better than  $0.1$   $\text{cm}^{-1}$ . The total time of spectrum collection was decreased to  $60$  s per point in the case of 2D mapping and the total acquisition times to collect all spectra for one map never exceeded  $8$  h.

An interferometric surface profiler with phase shift technology (Ade Phase Shift) and atomic force microscopy (Digital Instruments) were used to analyze the morphology of the deformation zones around impressions.

## III. RESULTS AND DISCUSSION

### A. Stokes and anti-Stokes Raman scattering of $\text{LaCoO}_3$

The Raman scattering response of pure  $\text{LaCoO}_3$  as a function of laser power is shown in Fig. 1. Four bands belonging to the cobaltite structure are observed at  $162$ ,  $448$ ,  $557$ , and  $673$   $\text{cm}^{-1}$ , in the case where the laser power is  $2.5$  mW. If the laser power increases to  $6.25$  mW, all four band positions shift to the lower wave numbers  $159$ ,  $442$ ,  $553$ , and  $665$   $\text{cm}^{-1}$ , respectively. With a further increase of the laser power to  $12.5$  mW, the position of the  $162$   $\text{cm}^{-1}$  mode softens further to  $156$   $\text{cm}^{-1}$  and the position of the  $448$   $\text{cm}^{-1}$  mode softens to  $430$   $\text{cm}^{-1}$ . At the same time the intensities of the two bands at  $557$  and  $673$   $\text{cm}^{-1}$  are significantly decreased and the bands become almost indistinguishable from

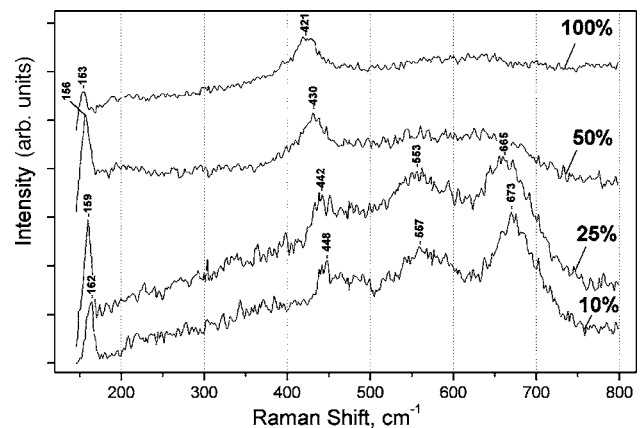


FIG. 1. Raman scattering of  $\text{LaCoO}_3$  perovskite at different laser intensities,  $100\%$  is  $25$  mW  $514.5$  nm  $\text{Ar}^+$  ion laser ( $\sim 155$   $\text{cm}^{-1}$ —rare earth internal vibration mode;  $\sim 430$   $\text{cm}^{-1}$ —O-O octahedral rotation;  $\sim 557$   $\text{cm}^{-1}$ —Co-O bending vibration;  $\sim 650$   $\text{cm}^{-1}$ —Co-O stretching vibration). All spectra are taken from the same selected location.

the background. At 100% of possible laser power (25 mW), the positions of the 162 and 448 modes soften up to 153 and 418  $\text{cm}^{-1}$ , respectively, and the bands at 557 and 673  $\text{cm}^{-1}$  almost completely vanish. If, following 25 mW spectrum collection, the laser power is decreased to 2.5 mW, two higher energy modes will reappear at their original positions at 557 and 673  $\text{cm}^{-1}$  and the two other mode positions will harden too. Such softening of the band positions indicates that there is a heating of the surface by the laser.

The 162  $\text{cm}^{-1}$  line can be tentatively assigned to the  $E_g$  mode [pure La internal vibration in the hexagonal (001)<sub>h</sub> plane]. The 448  $\text{cm}^{-1}$  line can possibly be assigned to the  $E_g$  mode (pure oxygen bending vibration). It should be noted that this band shows an extraordinary softening (from 448 to 416  $\text{cm}^{-1}$ ) upon heating by the laser. The assignment of the frequencies of the two broad Raman bands at 557 and 673  $\text{cm}^{-1}$  is unclear. These two bands were assigned to the calculated values for two  $E_g$  modes,<sup>18</sup> however, it was argued that these lines in rhombohedral  $\text{LaMnO}_3$  are not intrinsic for the ideal  $R\bar{3}c$  structure. In doped  $\text{La}_{1-x}\text{Sr}_x\text{MnO}_3$  the intensity of these lines decreases as the Sr content increases.<sup>19</sup> In  $\text{La}_{0.7}\text{Ca}_{0.3}\text{MnO}_3$  thin films, these lines are pronounced only in the Raman spectra of the insulating phase; they completely disappear in the metallic phase below the temperature of the metal-insulator transition.<sup>20</sup> It was assumed that the two modes under consideration are activated by Jahn-Teller local distortions that become “forbidden” in the rhombohedral symmetry, but local dynamic Jahn-Teller distortions are not forbidden by the space group symmetry. On the other hand, a transition from localized  $e$  to itinerant  $\sigma^*$  electrons would suppress any Jahn-Teller distortion associated with localized  $e$  electrons and would therefore wash out any modes associated with local dynamic Jahn-Teller distortions. A similar consideration can be taken into account for Raman scattering of the rhombohedral  $\text{LaCoO}_3$  perovskite since IS Co (III):  $t^5e^1$  is a Jahn-Teller ion. Therefore, alternatively the two 557 and 673  $\text{cm}^{-1}$  bands in  $\text{LaCoO}_3$  can also be assigned to local Jahn-Teller distortions in the semiconducting phase; the absence of these bands is an indication of the metallic state of the material in which localized  $e$  electrons have become transformed into itinerant  $\sigma^*$  electrons. The existence of monoclinic distortion also correlate well with the observed disappearance of two modes upon heating because the monoclinic phase exists only within the 50–500 K range.<sup>4</sup> The disappearance of the two broad peaks reflects the transition to a dynamically less distorted local structure in the metallic phase.

It is well known that anti-Stokes Raman scattering can be used to determine the temperature on the sample surface.<sup>21</sup> The temperature rise is affected by quantities such as power, stimulated surface area, exposure time, wavelength of laser radiation and the color, reflectivity, and thermal conductivity of the sample. For measurement with 25 mW laser power, an anti-Stokes band was observed for the 418  $\text{cm}^{-1}$  mode; therefore, the temperature on the surface of  $\text{LaCoO}_3$  was calculated from the Stokes and anti-Stokes Raman intensity ratio as follows:

$$T = 1.4387\omega_s \left\{ \ln \left( \frac{I_{St}}{I_{aSt}} \left[ \frac{\omega_L + \omega_s}{\omega_L - \omega_s} \right]^4 \right) \right\}^{-1}, \quad (1)$$

where  $I_{St}$  and  $I_{aSt}$  are the intensities of the Stokes and anti-Stokes Raman lines, respectively,  $\omega_s$  is the Raman shift,  $\omega_L$  is the absolute frequency of the laser line (19 435.2  $\text{cm}^{-1}$  for  $\text{Ar}^+$  ion laser), and  $T$  is the sample temperature in Kelvin. Equation (1) was derived from Ref. 21. The intensity ratio of the 418  $\text{cm}^{-1}$  mode of Stokes and anti-Stokes bands was calculated to be 2.63, and therefore the temperature on the cobaltite surface was raised to 528 K due to laser overheating during the collection of the Raman signal. The measured temperature (528 K) is slightly above the semiconductor-metal transition reported to be around 500 K for  $\text{LaCoO}_3$ .<sup>22</sup> At this temperature, the two broad bands disappeared. Therefore, it is another confirmation that if  $\text{LaCoO}_3$  has a metallic conductivity, the two broad bands at 557 and 673  $\text{cm}^{-1}$  vanish. A Jahn-Teller distortion is associated with localized  $e_g^1$  configurations, but not with itinerant electrons in a  $\sigma^*$  band of  $e$ -orbital parentage.

### B. Stress induced modifications of Raman spectra upon indentation in $\text{LaCoO}_3$

The influence of pressure on different physical properties of selected perovskites has been reported in a number of publications.<sup>23–25</sup> Pressure reduces the B-O band length of an  $\text{ABO}_3$  perovskite, and an increase in bandwidth can be achieved through contraction of the B-O bond length or straightening of the B-O-B bond angle.<sup>26</sup> It has been shown that the Mn-O distance decreases under pressure and the bending angle of the Mn-O-Mn bond opens in  $\text{La}_{1-x}\text{A}_x\text{MnO}_3$  perovskites. It was also reported that the application of pressure induces a metallic phase in  $\text{Pr}_{0.7}\text{Ca}_{0.3}\text{MnO}_3$ .<sup>27</sup> However, pressure would stabilize LS Co(III) relative to higher spin states in  $\text{LaCoO}_3$ .<sup>28,29</sup>

It is known that during the indentation of materials, reversible or nonreversible phase transformation and/or domain reorientation can take place.<sup>30–32</sup> A powerful method to identify the structural changes upon loading is Raman spectroscopy.<sup>33</sup> According to Ref. 34, the maximum contact stresses that arise at the interface between indenter and the material exist in the center of the Vickers indentation zone. This result, calculated in Ref. 34, is consistent with the optical image of the Vickers impression of  $\text{LaCoO}_3$  perovskite (Fig. 2), where one can see that the most dense damage zone exists in the center along the diagonals of the Vickers impression. Line mapping of Raman spectra reveals the pronounced difference between spectra taken from the center of the impression and all other points, both inside and outside of the impression (Fig. 2). While no 557 and 673  $\text{cm}^{-1}$  bands are observed on polished or cracked surfaces around the Vickers impression (the laser power was 25 mW), one can see that there is a pressure-induced enhancement of intensities of the 557 and 673  $\text{cm}^{-1}$  Raman bands in the center of the Vickers impression. The existence of these two bands is proof of the localized  $e$ -electron behavior of  $\text{LaCoO}_3$ ; therefore, one can expect that upon indentation, either a reversible

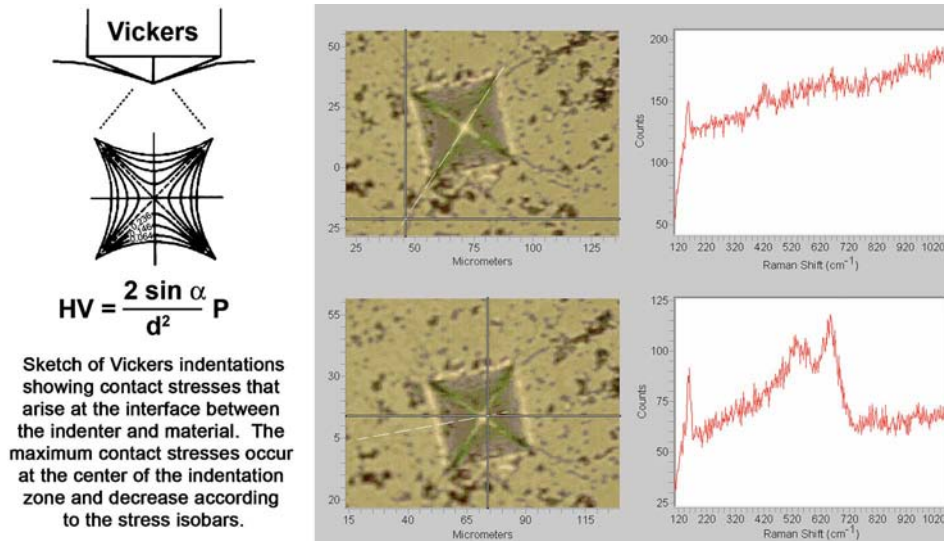


FIG. 2. (Color online) Optical micrographs and Raman spectra of Vickers impression of  $\text{LaCoO}_3$  perovskite. Crosshairs are shown at points of mapping.

semiconductor-metal-semiconductor or IS-LS-IS transition could occur. Upon loading, the material would transform to either the metallic or the LS state due to a significant pressure increase. However, upon unloading, a strong recovery of the cobaltite surface has been reported;<sup>35</sup> the recovery is accompanied by a reversal to the localized electron IS state. Therefore, in the center of the impression, where the maximum contact stresses are expected, the IS state of the perovskite with localized electrons occurs instead of the metallic state, and the 557 and 673  $\text{cm}^{-1}$  bands can be detected. A tensile stress stabilizes the state with the larger mean Co-O bond length.

Raman spectra of fractured, machined and scratched surfaces of  $\text{La}_{0.8}\text{Sr}_{0.2}\text{CoO}_3$  perovskite are shown in Fig. 3. It is well known that the fracture surface is the less deformed

surface where the stress level could be in the range of 80–100 MPa, while the surface scratched by a diamond cone is the most deformed surface where the stress level during the scratching could reach 1 GPa and above. While only three bands at 155, 407, and 560  $\text{cm}^{-1}$  could be detected at the fracture surface with no detectable broad band at 673  $\text{cm}^{-1}$ , the spectrum taken from the machined surface changes with a 603  $\text{cm}^{-1}$  broad band appearing after machining. At the same time the intensities of the Raman bands at 407 and 560  $\text{cm}^{-1}$  on the fracture surface changed drastically after applying high pressure during the scratching of the material surface. Not only has the intensity of the band at 560  $\text{cm}^{-1}$  been changed, but a broad band appears at 623  $\text{cm}^{-1}$  that possibly includes overlapping bands at 580 and 623  $\text{cm}^{-1}$ . The band at 407  $\text{cm}^{-1}$  can also be detected. These scratch results show that an irreversible change has occurred.

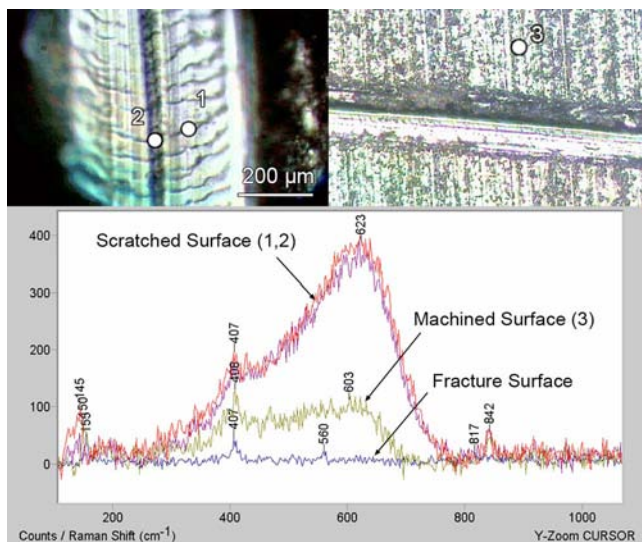


FIG. 3. (Color online) Optical micrographs of the scratched surface and Raman spectra of fractured, machined, and scratched surfaces of  $\text{La}_{0.8}\text{Sr}_{0.2}\text{CoO}_3$  perovskite.

### C. Stress induced deformation upon indentation in $\text{LaCoO}_3$

The nanoindentation of  $\text{LaCoO}_3$  perovskite revealed two interesting features: (1) an almost complete elastic recovery of the surface at small loading of 3–5 mN and (2) an elastoplastic response upon higher loads (for example, 600 mN) and large deformation zones around the impression that were observed after the indentation. During the indentation with the Berkovich sharp indenter, “pop-in” events could sometimes be observed on the loading part of the deformation curves. The large deformation zones can be detected either by phase shift optical microscopy (Fig. 4) or by an optical microscope with Nomarski contrast. Atomic force microscopy (AFM) can also be used to visualize the deformation zones (Fig. 5). As one can see from Fig. 5, there is a flat, smooth surface mapped by AFM far away from any impressions on the polished surface. The defects that can be seen on this surface are related to the grain pullout introduced during

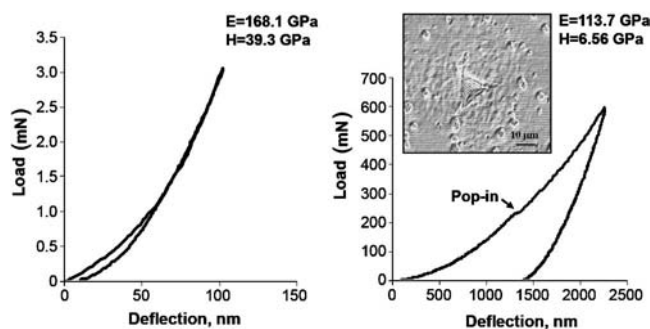


FIG. 4. Nanindentation of  $\text{LaCoO}_3$  perovskites with Berkovich diamond indenter. Young's modulus ( $E$ ) was measured to be 114 GPa, and hardness ( $H$ ) was measured to be 6.56 GPa. Deformation zones are observed around impression by phase shift optical microscopy.

the polishing of the material. However, the maps taken from the areas adjacent to the Vickers impression (areas A and B) clearly show a surface uplift. The size of the surface uplift is approximately  $1\text{--}2\ \mu\text{m}$ , which corresponds to the grain size of the  $\text{LaCoO}_3$  ceramics.

In recent years, stress analysis of ceramics using the so-called piezo-spectroscopic techniques, which includes Raman spectroscopy, has been reported.<sup>36–38</sup> Raman scattering wave numbers from solids are perturbed by elastic strain in the solid, and the perturbation is used as a tool for the non-destructive analysis of stress and strain. The analysis is based on the measurements of a peak shift of the Raman band where the material is subjected to a stress field. The frequency shift of the Raman bands is proportional to the mean stress averaged over the volume of the probed material. In most cases, a compressive uniaxial or biaxial stress results in the upshift of the Raman band to higher wave numbers and tensile stress produces a shift of the frequencies to lower wave numbers. However, there is no unique general relationship between the Raman spectrum parameters (particularly the wave number shift) and the stress.

The band position was determined to be at  $416\ \text{cm}^{-1}$  for the measurement taken from the polished, undeformed surface far away from the impression [Fig. 6(b)]. Both  $162$  and  $416\ \text{cm}^{-1}$  band positions (La internal vibration and O-O octahedral rotation, respectively) were found to be stress sensitive, the same as the broad band at  $673\ \text{cm}^{-1}$ . Therefore, any of these bands can be used for a band position fitting procedure. We have chosen the  $416\ \text{cm}^{-1}$  band because there is a sufficient background from both sides of the band to perform fitting efficiently and there is no overlapping with other bands that makes the fitting procedure complicated and the results ambiguous.

To analyze qualitatively residual stresses in  $\text{LaCoO}_3$  after the deformation, the area with a crack originating from the corner of the Vickers impression was selected to perform Raman mapping [Fig. 6(a)]. With the spectra of the  $416\ \text{cm}^{-1}$  band [Fig. 6(b)] collected from 678 points inside the selected area, a 2D Raman micrograph of the band positions was created. The image of the crack created with the Raman fitting procedure can be seen in the upper left corner of the optical micrograph. The blue color represents a downshift of

the O-O octahedral rotation band to lower wave numbers relative to the undeformed  $416\ \text{cm}^{-1}$  band position. This downshift corresponds to residual tensile stresses existing along the crack. At the same time, the points taken near the edge of the impression [such as Point I in Fig. 6(a)] show a strong upshift of the band positions with the point I being at  $422\ \text{cm}^{-1}$ , and some of the points being shifted to  $430\ \text{cm}^{-1}$ . Such an upshift is represented by the red color in the 2D Raman micrograph; it corresponds to the existence of a residual compressive stress. These results are in good agreement with a stress distribution around the Vickers indentation in  $\text{Si}_3\text{N}_4$  ceramics.<sup>37</sup> It was expected that the band inside of the impression would cause a shift of the band to a higher frequency that would correspond to the existence of a residual compressive stress, as was found for  $\text{Si}_3\text{N}_4$  and other ceramics. However, the  $416\ \text{cm}^{-1}$  band position was shifted to lower frequencies (point III in Fig. 6), which correspond to a residual tensile stress. These findings are in line with the nanoindentation results at small loads (3 mN) showing a strong elastic recovery of the perovskite surface. The schematic presentation of the indentation-induced deformation zones around a Vickers impression was created on the basis of the  $416\ \text{cm}^{-1}$  band shifts [Fig. 6(c)]. It is important to note that the compressive stress in the deformation zones between Vickers cracks could contribute to the small grain rotation that occurs upon Vickers loading and results in the surface uplift detected by the phase shift microscopy, AFM, and Nomarski (Figs. 4 and 5). Such stress-induced grain rotation has never been reported for  $\text{LaCoO}_3$  perovskites. The grain rotation can act as a new toughening mechanism in the ferroelastic cobaltites in addition to the well-known domain switching and phase transformation.<sup>39,40</sup>

#### IV. SUMMARY

Rhombohedral  $\text{LaCoO}_3$  perovskite is a Raman active material and can be studied by Raman spectroscopy. The four bands at  $162$ ,  $448$ ,  $557$ , and  $673\ \text{cm}^{-1}$  were generally observed where the laser power was reduced to  $2.5\ \text{mW}$  so as to give no overheating of the cobaltite surface. Softening of Raman modes is observed with an increase of laser power; for example, a  $448\ \text{cm}^{-1}$  band can soften up to the  $416\ \text{cm}^{-1}$  position. The semiconductor/metal transition along with a decrease in the rhombohedral distortion of  $\text{LaCoO}_3$  could be driven by laser induced overheating during collection of the Raman signal. With an increase of laser power up to  $25\ \text{mW}$ , the surface temperature of the cobaltites increases up to  $528\ \text{K}$  and two broad bands at  $557$  and  $673\ \text{cm}^{-1}$  disappear; this disappearance can be attributed to the metallic state of the material, which suppresses local Jahn-Teller distortions associated with a localized-electron  $\text{IS Co(III): } t^5e^1$  state. There are significant stress-induced changes in the Raman spectrum of  $\text{LaCoO}_3$  after indentation. The significant growth of two  $557$  and  $670\ \text{cm}^{-1}$  bands at the center of the impression was explained by a reversible transition upon loading and further unloading of the perovskite. Stabilization of the LS state under pressure would be reversible. The  $416\ \text{cm}^{-1}$  band was found to be stress sensitive and, there-

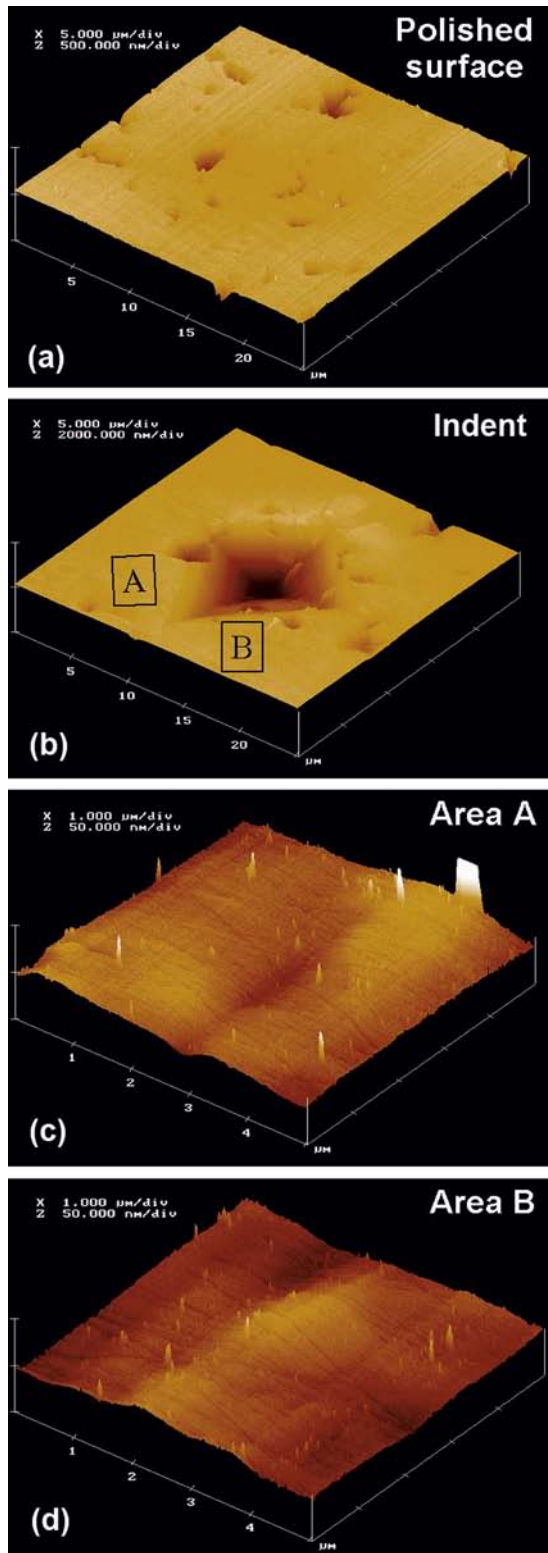


FIG. 5. (Color) AFM images of the polished surface (A), Vickers impression (B), and deformation zones around the impression (C) and (D). While no surface uplift could be found on the polished surface far from the indentation, the uplift surface with a size of 1–2 μm can be seen close to the Vickers impression [areas marked (A) and (B)]. A grain orientation can be one of the toughening mechanisms acting in LaCoO<sub>3</sub>.

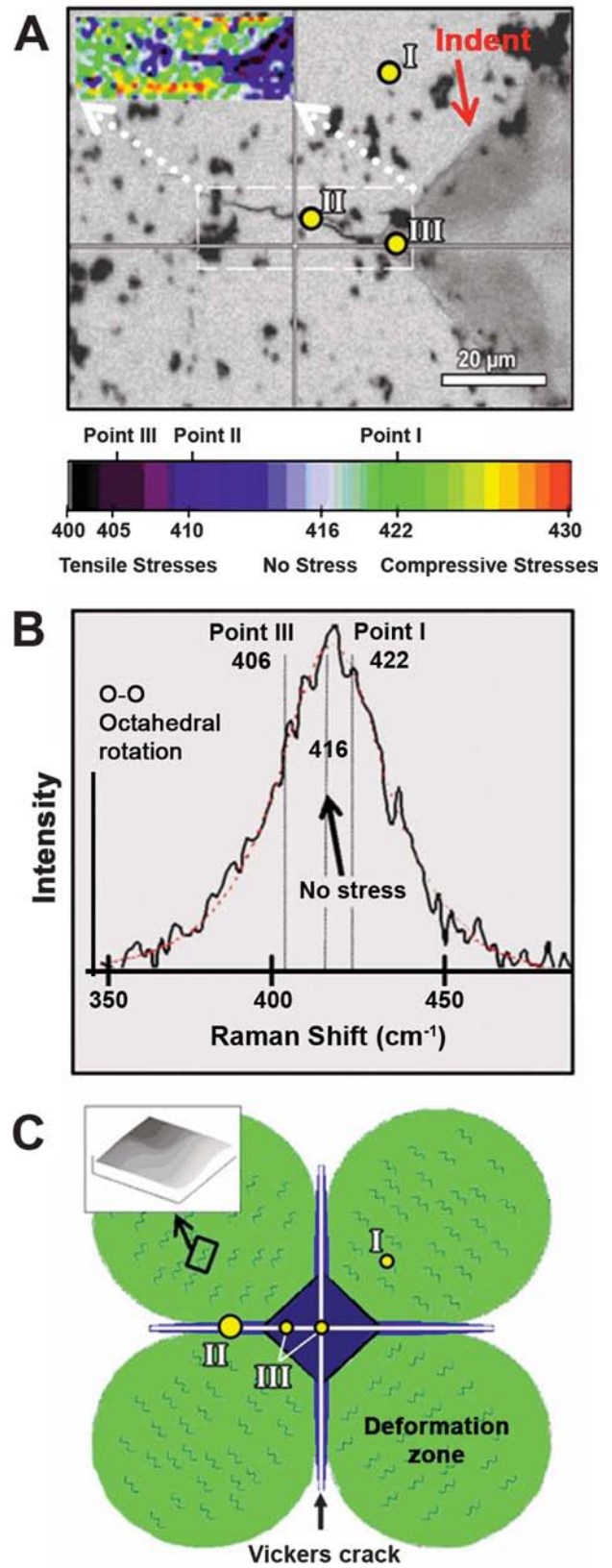


FIG. 6. (Color) (A) 2D Raman micrograph of a crack generated from the corner of Vickers impression; (B) O-O octahedral rotation band positions of LaCoO<sub>3</sub> spectrum; and (C) a schematic presentation of the indentation induced deformation zones around a Vickers impression.

fore, well suited for mapping of the residual stress distribution in the deformed cobaltites. A qualitative estimation of the residual stresses around Vickers indentation was done; residual tensile stresses were found to exist along corner cracks; and residual compressive stresses were distributed in the deformation zones inbetween cracks. A strong downshift of the  $416\text{ cm}^{-1}$  band, indicating the possible existence of residual tensile stress, was found inside the Vickers impression. A tensile stress would be relieved by reversal to the IS semiconductive state. A surface uplift was found, which is attributable to grain reorientation caused by the compressive

stress in the deformation zones, and such grain rotation can contribute to the toughening mechanisms of the ferroelastic  $\text{LaCoO}_3$  perovskites.

#### ACKNOWLEDGMENTS

The financial support of the National Science Foundation through Grant No. DMR-0201770 is acknowledged. This work was also partly performed at the Army Center for Nanoscience and Nanomaterials, North Carolina A&T State University.

\*Electronic address: nao22@drexel.edu

- <sup>1</sup>J. B. Goodenough and J.-S. Zhou, *Struct. Bonding* (Berlin) **98**, 17 (2001), and references therein.
- <sup>2</sup>S. Yan, J.-S. Zhou, and J. B. Goodenough (unpublished).
- <sup>3</sup>J.-P. Coutures, J. M. Badie, R. Berjoan, J. Coutures, R. Flamand, and A. Rouanet, *High. Temp. Sci.* **13**, 331 (1980).
- <sup>4</sup>G. Maris, Y. Ren, V. Volotchaev, C. Zobel, T. Lorenz, and T. T. M. Palstra, *Phys. Rev. B* **67**, 224423 (2003).
- <sup>5</sup>O. Van der Biest, T. Laoui, J. Vleugels, K. Sumanasiri, H. Mohrbacher, B. Blanpain, and J. P. Celis, *Corrosion of Advanced Ceramics*, edited by K. G. Nickel, NATO ASI Series (Kluwer Academic, Dordrecht, The Netherlands, 1994).
- <sup>6</sup>A. Ishikawa, J. Nohara, and S. Sugai, *Phys. Rev. Lett.* **93**, 136401 (2004).
- <sup>7</sup>S. Yoon, H. L. Liu, G. Schollerer, S. L. Cooper, P. D. Han, D. A. Payne, S. W. Cheong, and Z. Fisk, *Phys. Rev. B* **58**, 2795 (1998).
- <sup>8</sup>C. Roy and R. C. Budhani, *J. Appl. Phys.* **85**, 3124 (1999).
- <sup>9</sup>E. Granado, N. O. Moreno, A. Garcia, J. A. Sanjurjo, C. Rettori, I. Torriani, S. B. Oseroff, J. J. Neumeier, K. J. McClellan, S. W. Cheong, and Y. Tokura, *Phys. Rev. B* **58**, 11435 (1998).
- <sup>10</sup>V. Dediu, C. Ferdeghini, F. C. Maticotta, P. Nozar, and G. Ruani, *Phys. Rev. Lett.* **84**, 4489 (2000).
- <sup>11</sup>M. Popa, L. Van Hong, and M. Kakihana, *Physica B* **327**, 233 (2003).
- <sup>12</sup>V. P. Gnezdilov, A. V. Yeremenko, Yu. G. Pashkevich, P. Lemmens, G. Guntherodt, S. V. Shiryayev, G. L. Bychkov, and S. N. Barilo, *Low Temp. Phys.* **29**, 963 (2003).
- <sup>13</sup>A. M. Glazer, *Acta Crystallogr., Sect. B: Struct. Crystallogr. Cryst. Chem.* **28**, 3384 (1972).
- <sup>14</sup>M. V. Abrashev, A. P. Litvinchuk, M. N. Iliev, R. L. Meng, V. N. Popov, V. G. Ivanov, R. A. Chakalov, and C. Thomsen, *Phys. Rev. B* **59**, 4146 (1999).
- <sup>15</sup>H. Thomas and K. A. Muller, *Phys. Rev. Lett.* **21**, 1256 (1968).
- <sup>16</sup>W. Cochran and A. Zia, *Phys. Status Solidi* **25**, 273 (1968).
- <sup>17</sup>K. P. J. Williams, I. C. Wilcock, I. P. Hayward, and A. Whitley, *Spectroscopy* (Eugene, Or.) **11**, 45 (1996).
- <sup>18</sup>M. N. Iliev and M. V. Abrashev, *J. Raman Spectrosc.* **32**, 805 (2001).
- <sup>19</sup>V. B. Podobedov, A. Weber, D. B. Romero, J. P. Rice, and H. D. Drew, *Solid State Commun.* **105**, 589 (1998).
- <sup>20</sup>J. J. Neumeier, M. F. Hundley, J. D. Thompson, and R. H. Heffner, *Phys. Rev. B* **52**, R7006 (1995).
- <sup>21</sup>H. Fujimori, M. Kakihana, K. Ioku, S. Goto, and M. Yoshimura, *Appl. Phys. Lett.* **79**, 937 (2001).
- <sup>22</sup>P. Ravindran, P. A. Korzhavyi, H. Fjellvag, and A. Kjekshus, *Phys. Rev. B* **60**, 16 423 (1999).
- <sup>23</sup>D. N. Argyriou, J. F. Mitchell, J. B. Goodenough, O. Chmaissem, S. Short, and J. D. Jorgensen, *Phys. Rev. Lett.* **78**, 1568 (1997).
- <sup>24</sup>V. Laukhin, J. Fontcuberta, J. L. Garcia-Munoz, and X. Obradors, *Phys. Rev. B* **56**, R10 009 (1997).
- <sup>25</sup>J.-S. Zhou, J. B. Goodenough, A. Asamitsu, and Y. Tokura, *Phys. Rev. Lett.* **79**, 3234 (1997).
- <sup>26</sup>Y. Moritomo, A. Asamitsu, and Y. Tokura, *Phys. Rev. B* **51**, R16 491 (1995).
- <sup>27</sup>Y. Moritomo, H. Kuwahara, Y. Tomioka, and Y. Tokura, *Phys. Rev. B* **55**, 7549 (1997).
- <sup>28</sup>R. Lengsdorf, M. Ait-Tahar, S. S. Saxena, M. Ellerby, D. I. Khomskii, H. Micklitz, T. Lorenz, and M. M. Abd-Elmeguid, *Phys. Rev. B* **69**, 140403(R) (2004).
- <sup>29</sup>T. Vogt, J. A. Hriljac, N. C. Hyatt, and P. Woodward, *Phys. Rev. B* **67**, 140401(R) (2003).
- <sup>30</sup>A. Virkar and R. Matsumoto, *J. Am. Ceram. Soc.* **69**, c-224 (1986).
- <sup>31</sup>F. R. Chien, F. J. Uvic, V. Prakash, and A. H. Heuer, *Acta Mater.* **46**, 2151 (1998).
- <sup>32</sup>J. Gilman, *J. Mater. Res.* **7**, 535 (1992).
- <sup>33</sup>Y. Gogotsi, A. Kailer, and K. Nickel, *Mater. Res. Innovations* **1**, 3 (1997).
- <sup>34</sup>B. A. Galanov, *Sov. Appl. Mech.* **18**, 711 (1982).
- <sup>35</sup>N. Orlovskaya, Y. Gogotsi, M. Reece, B. Cheng, and I. Gibson, *Acta Mater.* **50**, 715 (2002).
- <sup>36</sup>Q. Ma and D. R. Clarke, *J. Am. Ceram. Soc.* **78**, 1433 (1993).
- <sup>37</sup>V. Sergo, G. Pezzotti, G. Katagiri, N. Muraki, and T. Nishida, *J. Am. Ceram. Soc.* **79**, 5419 (1996).
- <sup>38</sup>S. Maschio, E. Lucchuni, and V. Sergo, *J. Am. Ceram. Soc.* **82**, 3145 (1999).
- <sup>39</sup>N. Orlovskaya, N. Browning, and A. Nicholls, *Acta Mater.* **51**, 5063 (2003).
- <sup>40</sup>K. Kleveland, N. Orlovskaya, T. Grande, A.-M. Moe, M.-A. Einarsrud, M.-A. K. Breder, and G. Gogotsi, *J. Am. Ceram. Soc.* **84**, 2029 (2001).